Čerenkov radiation from a finite trajectory of electrons

T. Takahashi, T. Kanai, Y. Shibata, K. Ishi, and M. Ikezawa
Research Institute for Scientific Measurements, Tohoku University, Katahira, Aoba-ku, Sendai 980-77, Japan

T. Nakazato, M. Oyamada, S. Urasawa, and T. Yamakawa
Laboratory of Nuclear Science, Tohoku University, Mikamine, Taihaku-ku, Sendai 982, Japan

K. Takami, T. Matsuyama, K. Kobayashi, and Y. Fujita
Research Reactor Institute, Kyoto University, Kumatori, Osaka 590-04, Japan
(Received 11 April 1994)

Properties of radiation emitted by relativistic electrons traveling through a limited trajectory of length L in helium and nitrogen gas at various pressures are experimentally investigated in the visible and the millimeter-wave regions. The radiation was generated by short bunches of electrons from a linear accelerator. In the long-wavelength region the Čerenkov threshold was blotted out, and the observed radiation showed characteristics of transition radiation even if the Čerenkov criterion $\beta n > 1$ was fulfilled. An alternative criterion $\beta(n - \lambda/L) > 1$ is proposed on the basis of the consideration of the formation zone.

PACS number(s): 41.60.Bq, 41.75.Ht, 42.72.Ai

I. INTRODUCTION

In a dielectric medium, Čerenkov radiation is emitted [1] when the velocity of a charged particle v exceeds that of light c/n, i.e., $\beta n > 1$, where n is the refractive index of the medium and $\beta = v/c$. The condition $\beta n > 1$ is called the Čerenkov criterion. For a medium of infinite extent, the propagation of radiation is confined in the direction of the Čerenkov angle θ_c which is defined by $\cos\theta_c = 1/\beta n$, that is, the angular distribution of radiation is given by the Dirac delta function of the type $\delta(\theta - \theta_c)$. The radiation is not emitted when $\beta n < 1$. The equation $\beta n = 1$ is called the Čerenkov threshold, which is defined in a medium of infinite extent.

The condition of the infinite extent of a medium is not practical. In actual experiments a trajectory of charged particles is limited by some kind of boundary, such as the windows in the Čerenkov counter. The theory of Čerenkov radiation emitted from a finite region was first derived by Tamm [2], in which it was shown that the intensity of radiation remained even if $\beta n < 1$. Lawson [3] and Zrelov *et al.* [4,5] made numerical calculations of the angular distribution on the basis of Tamm's theory in both cases of $\beta n > 1$ and $\beta n < 1$, and discussed the sharpness of the Čerenkov threshold. In the visible region experimental studies of the Čerenkov counter [6] verified that the radiation intensity did not vanish at gas pressures below the Čerenkov threshold. The remaining radiation was qualitatively considered to be transition radiation emitted from windows of the counter, because the observed intensity was independent of the path length. Transition radiation is emitted when an electron travels across an interface between two media with different dielectric constants, and was first theoretically studied by Frank and Ginzburg [7].

In the long-wavelength region some research groups have recently observed the radiation from a finite trajectory of electrons in a gas [8–12]. Through these experiments a problem about the nomenclature of the radiation in a gas has been introduced. The observed radiation was somewhat arbitrarily called Čerenkov radiation [8–10] or transition radiation [11,12], according to conventional nomenclature or to the property of radiation, respectively. This problem arises from the fact that the observed radiation can be analyzed by either the theory of Čerenkov or transition radiation. Therefore it appears significant for us to investigate the relation between Čerenkov and transition radiation, and to understand the role of the Čerenkov threshold for a finite length of the electron trajectory.

In this paper we describe our experimental results on the characteristics of the radiation emitted from a finite trajectory of electrons and discuss the practical meaning of the Čerenkov threshold. The radiation in helium and nitrogen gas at various pressures near around the Čerenkov threshold was observed in the visible and the millimeter-wave regions. To ensure the results, we used electron beams of two different linear accelerators, i.e., the Tohoku Linac at Tohoku University (150-MeV electron beam) and the KURRI Linac at Research Reactor Institute, Kyoto University (40-MeV electron beam). On the basis of the results of our experiments and from consideration of the formation zone, we propose an alternative criterion for Čerenkov radiation.

II. THEORY OF ČERENKOV AND TRANSITION RADIATION

For the formulation of Čerenkov and transition radiation, we consider an electron trajectory in a gas with the refractive index n, which is limited by a metallic window

(W) and a metallic mirror (M) with the mutual complex dielectric constant ϵ, as shown in Fig. 1.

According to Tamm's theory [2], the intensity of Čerenkov radiation from a finite trajectory (L) of an electron is given by [4]

$$\frac{d^2P_0}{d\Omega\, d\lambda} = \frac{\alpha n}{\lambda}\left(\frac{L}{\lambda}\right)^2 \left(\frac{\sin X(\lambda,\theta)}{X(\lambda,\theta)}\right)^2 \sin^2\theta, \tag{2.1}$$

$$X(\lambda,\theta) = \frac{\pi L}{\beta\lambda}\left(1-\beta n\cos\theta\right), \tag{2.2}$$

where α is the fine-structure constant, λ a wavelength in vacuum, β the ratio of the velocity of the electron to that of light, and θ the angle between a direction of observation and the electron trajectory. The intensity is represented by the number of photons (P_0) per unit wavelength ($d\lambda$) and unit solid angle ($d\Omega$). The observation point is assumed to be far from the radiation source. Equation (2.1) shows that the radiation intensity is not extinguished and remains finite even if $\beta n < 1$. When $|\beta n - 1|L/\lambda \gg 1$, Eq. (2.1) is integrated over all solid angles in two cases. For $\beta n > 1$,

$$\frac{dP_0}{d\lambda} = \frac{2\pi\alpha L}{\lambda^2}\left(1-\frac{1}{\beta^2 n^2}\right) + \frac{2\alpha}{\pi n\lambda}\left(\frac{1}{\beta n}\ln\frac{1+\beta n}{|1-\beta n|} - 2\right), \tag{2.3}$$

and for $\beta n < 1$,

$$\frac{dP_0}{d\lambda} = \frac{2\alpha}{\pi n\lambda}\left(\frac{1}{\beta n}\ln\frac{1+\beta n}{1-\beta n} - 2\right). \tag{2.4}$$

The first term of Eq. (2.3) represents the intensity of "pure" Čerenkov radiation from a continuous medium and it is proportional to L. Equation (2.4) and the second term of Eq. (2.3) result from the ends of the trajectory. In Tamm's theory the electron is assumed to have a constant velocity βc only during traveling the length L. Since this condition corresponds to the trajectory limited by perfect conductors on both sides, origin of the radiation given by Eq. (2.4) and the second term of Eq. (2.3) should be due to transition radiation, as is explicitly shown below.

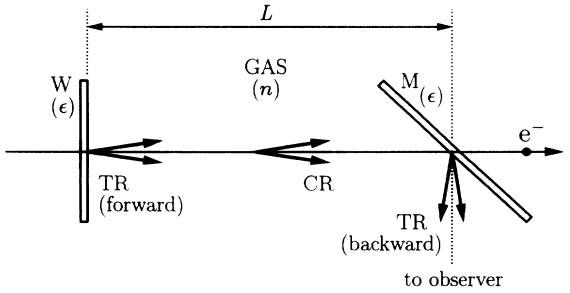

FIG. 1. The schematic view of radiation from an electron trajectory (e^-) limited by a metallic window (W) and a metallic mirror (M) with the mutual dielectric constant ϵ. The trajectory is in a gas with the refractive index n. Arrows with CR and with TR denote Čerenkov radiation and transition radiation, respectively.

Transition radiation is emitted from an interface of two media. With the experimental configuration shown in Fig. 1, the transition radiation from a metal-to-gas interface at the window (W), which is called the forward transition radiation, and from a gas-to-metal interface at the mirror (M), which is called the backward one, are observed. The intensity P_0^{FT} of the forward transition radiation is given by [13]

$$\frac{d^2P_0^{FT}}{d\Omega\, d\lambda} = \frac{\alpha\beta^2 n\sin^2\theta\cos^2\theta}{\pi^2\lambda(1-\beta^2n^2\cos^2\theta)^2}|\zeta|^2, \tag{2.5}$$

$$\zeta = \frac{(\epsilon-n^2)[1-\beta^2n^2-\beta(\epsilon-n^2\sin^2\theta)^{1/2}]}{[\epsilon\cos\theta+n(\epsilon-n^2\sin^2\theta)^{1/2}][1-\beta(\epsilon-n^2\sin^2\theta)^{1/2}]}. \tag{2.6}$$

The expression of the backward transition radiation is obtained from Eq. (2.5) multiplied by the Fresnel coefficient of reflection at the surface of the mirror (M) and replaced β by $-\beta$. When $|\epsilon| \gg 1$, the factor $|\zeta\cos\theta|^2$ is close to unity, and this approximation is satisfied by most metals in the long-wavelength region. Aluminum, for example, satisfies this condition even in the visible region, because its plasma frequency is in the vacuum ultraviolet region [14]. When both the window (W) and the mirror (M) are such a type of conductor, the intensity of transition radiation which propagates to an observer in Fig. 1 is given by [15,16]

$$\frac{d^2P_0^T}{d\Omega\, d\lambda} = \frac{2\alpha\beta^2 n\sin^2\theta}{\pi^2\lambda(1-\beta^2n^2\cos^2\theta)^2}\left(1-\cos\frac{2\pi L}{L_f}\right), \tag{2.7}$$

where L_f is the length of the formation zone and is given by [17]

$$L_f = \frac{\beta\lambda}{|1-\beta n\cos\theta|}. \tag{2.8}$$

The definition of the formation zone is different by a factor of 2π in the literature [4,17]. In our previous work [16], there was a factor of 2π in the denominator.

When $|\beta n-1|L/\lambda \gg 1$, the result of integration of Eq. (2.7) over all solid angles is written as

$$\frac{dP_0^T}{d\lambda} = \frac{2\alpha}{\pi n\lambda}\left\{\frac{1+\beta^2n^2}{2\beta n}\ln\frac{1+\beta n}{|1-\beta n|} - 1\right\}. \tag{2.9}$$

For the medium of a gas ($n \simeq 1$) and for a high-energy electron ($\beta \simeq 1$), Eq. (2.4) or the second term of Eq. (2.3) derived for Čerenkov radiation from a finite trajectory and Eq. (2.9) derived for transition radiation are approximately reduced to the same functional form

$$\frac{dP_0^T}{d\lambda} = \frac{2\alpha}{\pi\lambda}\ln\frac{2}{|1-\beta n|}. \tag{2.10}$$

Thus it is shown that the intensity of Eq. (2.1) which is

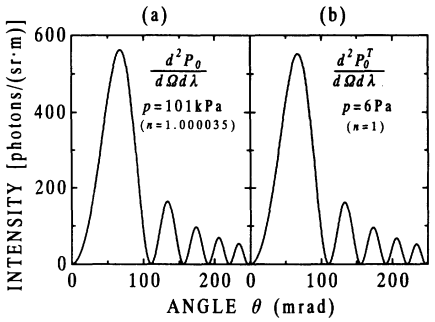

FIG. 2. The calculations of the angular distribution of (a) the radiation from a limited trajectory of an electron and (b) transition radiation. The energy of the electron is assumed to be 150 MeV, the wavelength $\lambda = 1$ mm, and the length of path $L = 165$ mm.

derived for Čerenkov radiation includes not only "pure" Čerenkov radiation but also transition radiation from both metal-to-gas and gas-to-metal interfaces.

When $|\beta n - 1|L/\lambda \gg 1$ is not fulfilled, integration of Eq. (2.1) cannot be distinctly divided in two terms of Čerenkov and transition radiation. For $n \simeq 1$, $\beta \simeq 1$, and a small angle θ, i.e., $|\beta n - 1|L/\lambda \ll 1$, Eq. (2.1) is smoothly continuous at the Čerenkov threshold $\beta n = 1$ when n is varied, and the sharp edge of discontinuity does not appear [3]. Then, Eq. (2.1) of the radiation from a finite length and Eq. (2.7) of transition radiation have approximately the same functional form and the same angular distribution:

$$\frac{d^2P_0}{d\Omega\, d\lambda} \simeq \frac{d^2P_0^T}{d\Omega\, d\lambda} \simeq \frac{\alpha n}{\lambda^3} L^2 \sin^2\theta. \tag{2.11}$$

As an example, Fig. 2(a) shows the theoretical intensity calculated by Eq. (2.1) for $\lambda = 1$ mm, $L = 165$ mm, a 150-MeV electron beam, and helium gas at atmospheric pressure which is above the Čerenkov threshold. Then, the value of $|\beta n - 1|L/\lambda$ is about 0.005. The intensity represents the number of photons per unit solid angle (sr) and unit wavelength (m). The angular distribution of Eq. (2.7) for transition radiation in vacuum ($n = 1$) is shown in Fig. 2(b). These two angular distributions are the same, though the theories for the derivations of the two equations are different. One is Eq. (2.1) for Čerenkov radiation with transition radiation and the other is Eq. (2.7) for only transition radiation. In other words, Eq. (2.1) mostly represents the intensity of transition radiation in the long-wavelength region, even if the Čerenkov criterion $\beta n > 1$ is fulfilled. This aspect of Eq. (2.1) has introduced an ambiguity about the nomenclature of the radiation emitted in a gaseous medium in the long-wavelength region [8–12]. Therefore another criterion of Čerenkov radiation is necessary.

III. EXPERIMENTAL PROCEDURES

A. Generation of radiation

The Čerenkov threshold is determined by the refractive index of a gas and the velocity of an electron beam. Two combinations of gases and electron beams were employed. Experiments were performed at facilities of the Tohoku Linac and the KURRI Linac. The experimental conditions of the two linacs, i.e., the electron-beam energy, the energy spread, the accelerating radio frequency, the duration of a burst, and the repetition rate, are shown in Table I. The average beam current is a typical value during the experiment and is proportional to the number of electrons in the bunch. The current was measured by a secondary emission monitor at the Tohoku Linac and by a Faraday cup at the KURRI Linac.

The arrangement of the experiment is shown in Fig. 3. The chamber was filled with gas at various pressures. The characteristics of two kinds of gases are listed in Table II. The gases were kept at room temperature. In this paper we designate the gas pressure of 101 kPa as atmospheric pressure, and both 6 Pa at the Tohoku Linac and 10 Pa at the KURRI Linac as vacuum. The electron trajectory was limited by an aluminum foil 15 μm thick and by a mirror ($M1$). In the millimeter-wave region, a flat aluminum foil 15 μm thick was used as the mirror ($M1$). In the visible region it was replaced with an aluminum-coated-silica glass 0.3 mm thick. In the wavelength range of our experiment aluminum was regarded as a perfect conductor [14]. When the angular distribution of radiation was observed, the mirror ($M1$) was rotated around a vertical axis. The distance L between the foil and the mirror ($M1$) was varied by moving the foil when the dependence of the intensity on the length L was observed. In order to cut off the radiation emitted from a titanium window ($W2$), some sheets of absorber of far-infrared radiation (Eccosorb AN72, Emerson & Cuming Co.) were put around the aluminum foil.

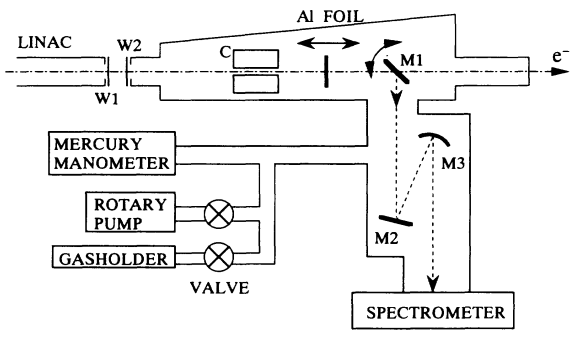

FIG. 3. The arrangement of the experiment. Keys are $W1$, $W2$, titanium windows 20 μm thick; C, a beam collimator; $M1$, $M2$, $M4$, plane mirrors; $M3$, a spherical mirror; and e^-, electron beam. The beam collimator (C) is a cylinder of aluminum 100 mm in diameter and 120 mm long with a central hole 12 mm in diameter, and is used only at the KURRI Linac. The vacuum chamber is evacuated, or filled with He or N_2 gas at various pressures. As the mirror ($M1$), a flat aluminum foil 15 μm thick is used in the millimeter-wave region and an Al-coated-silica glass 0.3 mm thick is used in the visible region. The detector is a Si bolometer in the millimeter-wave region and a photomultiplier tube in the visible region. A grating-type spectrometer for the visible region is placed behind the exit slit of the far-infrared spectrometer.

TABLE I. The experimental conditions of the electron beam.

	Tohoku Linac	KURRI Linac
Electron energy (MeV)	150	40
Energy spread (%)	0.2	167
Accelerating rf (GHz)	2.856	1.300
Duration of a burst (μs)	2	0.033
Repetition rate (pulses/s)	150	55
Average beam current (μA)	0.5	1.5
Number of electrons per bunch	3.6×10^6	4.0×10^9

The electron beam of the KURRI Linac has a large transverse size of a few centimeters in diameter. In order to diminish this size, a beam collimator of cylindrical aluminum (C in Fig. 3) whose size was 120 mm long and 100 mm in diameter was used. It had a central hole of 12 mm in diameter and was set at a distance of 320 mm upstream from the mirror ($M1$). The influence of the collimator on the observed radiation was eliminated by some sheets of Eccosorb around the aluminum foil. The collimator was not used for the electron beam of the Tohoku Linac.

The profile of the electron beams at the position of the aluminum foil in Fig. 3 is summarized in Table III. The longitudinal length of the bunch was estimated from the spectrum of coherent synchrotron radiation [10,18]. The transverse size and the angular divergence were estimated on the basis of the multiple scattering of electrons by the titanium windows and by gas in the chamber [19]. The calculated values of the normalized emittance ε_n which is defined in the Appendix are of the order of 10^{-3} m rad as are shown in Table III. Compared with these values, the normalized emittance of the electron beam of the linear accelerator is negligibly small, for example, about $7 \times 10^{-5}\pi$ m rad at the Tohoku Linac [20].

B. Detection of radiation and calibration

The radiation was reflected by a plane mirror ($M2$ in Fig. 3), collected by a spherical mirror ($M3$), and was led to a grating-type far-infrared spectrometer [18]. The acceptance angle of radiation by the mirror ($M3$) is 70 mrad at the Tohoku Linac and 100 mrad at the KURRI Linac. Millimeter-wave radiation was detected by a liquid-helium-cooled silicon bolometer. When visible light was observed, a grating-type spectrometer for the visible region (Shimadzu Co.) with a glass filter was used. Visible light was detected by a photomultiplier tube (R1508, Hamamatsu Photonics K.K.).

TABLE II. The characteristics of the radiation source.

	Tohoku Linac	KURRI Linac
Gas	He	N_2
Refractive index[a]	$1 + 3.50 \times 10^{-5}$	$1 + 2.97 \times 10^{-4}$
Pressure of gas	6 Pa–101 kPa	10 Pa–101 kPa
Radiator length L	75–440 mm	61–300 mm

[a]The values at 101 kPa.

In the millimeter-wave region the absolute sensitivity of the measuring system was calibrated by blackbody radiation emitted from a graphite cavity at a temperature of 1200 K [18]. In the visible region a standard halogen lamp of 500 W (Ushio Inc.) was used for the calibration.

The accuracy of the observed intensity in this experiment was estimated to be within a factor of 1.5.

IV. EXPERIMENTAL RESULTS

In this section experimental results in the visible and the millimeter-wave region are described. In the millimeter-wave region coherent radiation was observed due to short bunches of electrons. The intensity of the observed radiation was proportional to the square of the beam current, i.e., to the square of the number of electrons in the bunch. The quadratic dependence is a property of coherent radiation as described in the Appendix where the theory of the coherence effect is explained. In this section theoretical calculations of Čerenkov and transition radiation in the millimeter-wave region are performed by substituting Eq. (2.1) or Eq. (2.7) into P_0 in Eq. (A2) of coherent radiation.

A. Dependence of radiation intensity on pressure of gas

The relation between the pressure of gas and the intensity along the electron trajectory ($\theta = 0$ rad) is shown in Figs. 4(a) and 4(b). The gas and the energy of electrons were (a) helium gas and 150 MeV at the Tohoku Linac, and (b) nitrogen gas and 40 MeV at the KURRI Linac. The refractive index n of gas is related with a gas pressure p as $n = \sqrt{1 + kp}$, where k is a constant. The pressure p_{thr} at the Čerenkov threshold $\beta n = 1$ is (a) 16.8 kPa and (b) 27.8 kPa, which is shown by the dotted line and the arrow in Figs. 4(a) and 4(b).

The open circles show the observed values at $\lambda = 500$ nm and the solid circles $\lambda = 1$ mm [or 2 mm for (b)]. The intensity is normalized by the value in vacuum. The length L, which is the distance between the foil and the mirror ($M1$) in Fig. 3, is (a) 165 mm and (b) 156 mm. The values of L/λ for the millimeter-wave region are three orders of magnitude smaller than ones for the visible region and the condition $|\beta n - 1|L/\lambda \gg 1$ is not fulfilled. The observed intensity at $\lambda = 500$ nm steeply increases with pressure around the pressure of the Čerenkov

TABLE III. The spatial parameters of the bunch at the position of the aluminum foil.

	Tohoku Linac		KURRI Linac	
	101 kPa	6 Pa	101 kPa	10 Pa
Transverse size 2σ (mm)	7.1	7.0	18	15
Angular divergence 2Ψ (mrad)	4.9	4.6	35	18
Normalized emittance ε_n (m rad)	$2.6 \times 10^{-3}\pi$	$2.4 \times 10^{-3}\pi$	$1.2 \times 10^{-2}\pi$	$5.3 \times 10^{-3}\pi$
Longitudinal bunch length (mm)		0.25		14

threshold. The factor of enhancement at atmospheric pressure compared with the value in vacuum is (a) about 30 and (b) about 900. This enhancement is due to the generation of Čerenkov radiation. On the other hand, the intensity at $\lambda = 1$ or 2 mm shows no distinct change over pressures below and above the threshold. Thus Čerenkov radiation was not observed in the millimeter-wave region.

The dashed and the broken curves show the theoretical intensity calculated by Eq. (2.1) for $\lambda = 500$ nm and $\lambda =$ 1 mm [or 2 mm for (b)], respectively. These calculated values are in good agreement with the observed ones.

B. Angular distribution of radiation

The experimental results of the angular distribution of radiation for $\lambda = 1$ mm and $L = 165$ mm at the Tohoku Linac are shown in Fig. 5. The intensity shows the number of photons integrated over the acceptance angle of 70 mrad, per bandwidth of 1% (i.e., $\Delta\lambda/\lambda = 0.01$), and at the average beam current of 0.5 μA. The solid and the broken curves represent the observed data at atmospheric pressure and in vacuum, respectively. The angle at the maximum intensity is about 45 mrad.

When $|\beta n - 1|L/\lambda \gg 1$, for example, in the visible region $|\beta n - 1|L/\lambda \sim 10$, the direction of propagation of the Čerenkov radiation is centered around the Čerenkov angle θ_c (= 7.6 mrad for a 150-MeV electron beam), whereas the transition radiation is centered around $1/\gamma$ ($= \sqrt{1-\beta^2} = 3.4$ mrad). In the millimeter-wave region, however, the value of $|\beta n - 1|L/\lambda$ is about 0.005 and the condition $|\beta n - 1|L/\lambda \gg 1$ is not fulfilled. The angular distributions of both types of radiation broaden and show the same form as shown in Figs. 2(a) and 2(b) in Sec. II.

The dotted curve in Fig. 5 shows the calculation of coherent Čerenkov radiation from a limited trajectory by Eq. (2.1) integrated over the acceptance angle of 70 mrad. The calculated intensity of coherent transition radiation by Eq. (2.7) overlaps with this dotted curve. The results of observation and the calculations in Fig. 5 are in good agreement. The angular distribution of the observed radiation at atmospheric pressure shows that of transition radiation.

C. Dependence of radiation intensity on length of trajectory

Figures 6(a) and 6(b) show the relation between the intensity in the direction of $\theta = 0$ rad and the length L of the electron trajectory which is the distance between the aluminum foil and the mirror, at the Tohoku Linac (a) and the KURRI Linac (b). The intensity is normalized to the value of $L = 165$ mm (a) and of $L = 156$ mm (b). The solid circles represent the observed values for

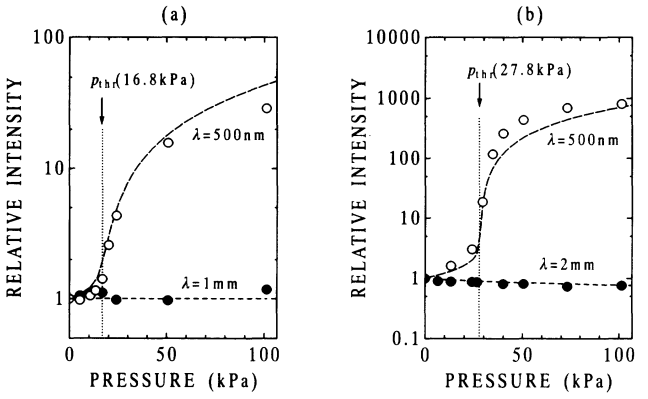

FIG. 4. The relation between the intensity and the pressure; (a) He gas and the 150-MeV electron beam; (b) N_2 gas and the 40-MeV electron beam. The open and the solid circles show the observed intensity in the visible and the millimeter-wave region, respectively. The dashed and the broken curves show the theoretical intensity for the respective wavelengths. The intensity is normalized to that in vacuum. The pressure of the Čerenkov threshold p_{thr} is (a) 16.8 kPa and (b) 27.8 kPa.

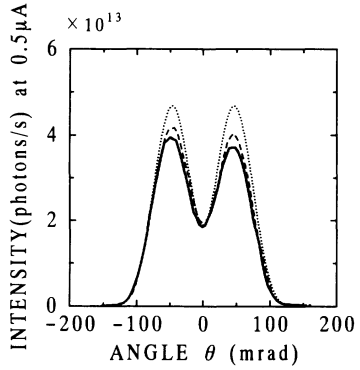

FIG. 5. The angular distribution of radiation at $\lambda = 1$ mm from the Tohoku Linac. The solid and broken curves show the observed data at atmospheric pressure and in vacuum, respectively. The dotted curve is the theoretical intensity integrated over the acceptance angle of 70 mrad.

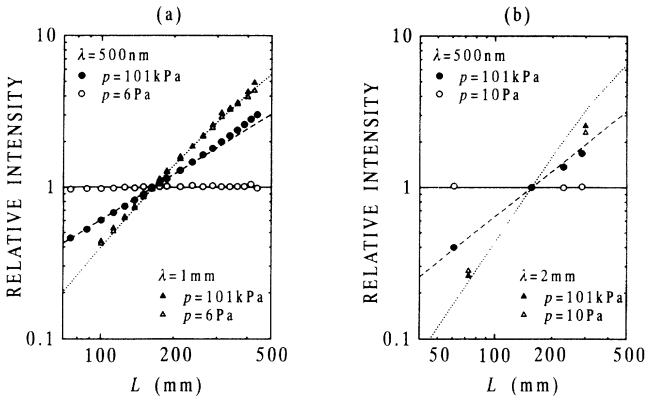

FIG. 6. The relation between the intensity and the length of the trajectory of (a) the 150-MeV electron beam and (b) the 40-MeV electron beam. The intensity is normalized to the value of (a) $L = 165$ mm and (b) $L = 156$ mm. The solid and the open circles represent the observed intensity in the visible region at atmospheric pressure and in vacuum, respectively. The solid and the open triangles represent the values in the millimeter-wave region at the respective pressures. The solid and the broken curves are the calculations at $\lambda = 500$ nm at the respective pressures. The dotted curve represents calculated values at the two pressures in the millimeter-wave region.

$\lambda = 500$ nm at atmospheric pressure. The intensity is proportional to L and shows the property of Čerenkov radiation from the medium, as expressed by the first term of Eq. (2.3). The broken curve is the theoretical intensity calculated by Eq. (2.1) using the parameters of the experiment, and is in good agreement with the observed data.

The open circles represent the observed values for $\lambda = 500$ nm in vacuum. The observed radiation is transition radiation and the intensity in the short-wavelength region is independent of L as expressed by Eq. (2.9). The solid curve is the theoretical intensity calculated by Eq. (2.1) using the parameters of the experiment. The observed data are consistent with the theoretical calculation.

In the millimeter-wave region the length of the formation zone L_f is much longer than the length L in this experiment. For example, the values of L_f at the two pressures, when the direction of radiation is parallel to the electron trajectory ($\theta = 0$ rad), are shown in Table IV. When L is much shorter than the length L_f of the formation zone, the term $1-\cos(2\pi L/L_f)$ in Eq. (2.7) for transition radiation is approximated as $2\pi^2 L^2/L_f^2$ and the intensity shows the quadratic dependence on L [16,24]. The solid and the open triangles in Fig. 6 represent, respectively, the observed values at atmospheric pressure and in vacuum in the millimeter-wave region, (a) $\lambda = 1$ mm and (b) $\lambda = 2$ mm. The observed intensities at both pressures have almost the same dependence on L and they are nearly proportional to the square of L. The dotted curve shows the calculated intensity of Eq. (2.1). The calculation of transition radiation by Eq. (2.7) overlaps with this curve.

Thus the quadratic dependence of the intensity on the length L shows that the observed radiation is transition radiation in the millimeter-wave region even at atmospheric pressure where the condition $\beta n > 1$ is fulfilled. The gradients of the calculated curves in Figs. 6(a) and 6(b) are slightly smaller than 2 at large values of L. This is caused by the fact that the effective acceptance angle decreases at large values of L.

TABLE IV. The length L_f of the formation zone for $\theta = 0$ rad.

	Tohoku Linac		KURRI Linac	
Wavelength	101 kPa	6 Pa	101 kPa	10 Pa
500 nm	17.1 mm	86.2 mm	2.32 mm	6.13 mm
1 mm	34.2 m	172 m		
2 mm			9.29 m	24.5 m

D. Spectrum of radiation

Figures 7(a) and 7(b) show additional data of the spectra along the electron trajectory ($\theta = 0$ rad) in the visible and the millimeter-wave regions at the Tohoku Linac and the KURRI Linac, respectively. The intensity represents the number of photons per second, per bandwidth of 1% (i.e., $\Delta\lambda/\lambda = 0.01$), and at the average beam current of each linac.

The solid and the broken curves in the millimeter-wave region show the observed spectra of coherent radiation at atmospheric pressure and in vacuum, respectively. The spectra at both pressures are nearly the same, and in Fig. 7(a) these almost overlap each other. The spectra show peaks at (a) $\lambda = 1$ mm and (b) $\lambda = 3$ mm. The difference between the observed spectra at the two linacs is due to the difference of the bunch shape according to the theory of coherent radiation in the Appendix.

The solid and the open circles in the visible region are observed values at the wavelength of 500 nm. The ratio of the intensity at atmospheric pressure to that in vacuum is about 30 in (a) and about 900 in (b). These values of the ratios are in agreement with the observed results of the dependence of the radiation intensity on the gas pressure, which are described in Sec. IV A.

The dashed and the dotted curves, respectively, represent the calculated intensity by Eq. (2.1) for atmospheric pressure and by Eq. (2.7) for vacuum, which are integrated over the acceptance angle and over the electron numbers of the average beam current. These curves represent incoherent radiation. As described in Sec. II, Eq. (2.1) expresses the total intensity of both Čerenkov and transition radiation, and Eq. (2.7) expresses only the intensity of transition radiation.

In the millimeter-wave region the observed intensity at the maximum peaks is enhanced by a factor of about 4×10^6 in Fig. 7(a) and about 2×10^6 in Fig. 7(b) in comparison with the calculated intensity of incoherent radiation. The factor for the Tohoku Linac is close to the number of electrons per bunch 3.6×10^6 and this is a property of coherent radiation. The factor for the KURRI Linac is three orders of magnitude smaller than

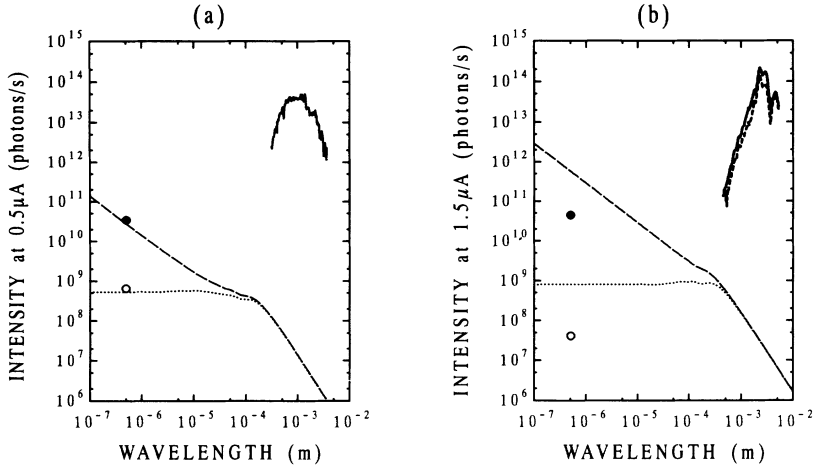

FIG. 7. The observed spectra of radiation from (a) the 150-MeV electron beam and (b) the 40-MeV electron beam. The intensity shows the number of photons per second per bandwidth of 1% (i.e., $\Delta\lambda/\lambda = 0.01$) and at the average beam current. The solid and the broken curves in the millimeter-wave region and the solid and the open circles in the visible region show the intensity of the observed radiation at atmospheric pressure and in vacuum, respectively. The dashed and the dotted curves show the theoretical intensity at respective pressures.

the number of electrons per bunch 4.0×10^9. The small value is considered to be attributed to the decrease of the coherence effect due to large dimensions of the bunch compared with the wavelength, as shown in Table III.

In the visible region the observed values at both pressures are in good agreement with the theoretical calculation of the incoherent radiation at the Tohoku Linac in Fig. 7(a). At the KURRI Linac in Fig. 7(b) the absolute intensity of the observed radiation at each pressure is different from the calculation by an order of magnitude, though the ratio of the intensity at atmospheric pressure to that in vacuum is in good agreement with the calculation. The reason for this discrepancy of the absolute values was probably due to an inaccurate gain of the preamplifier of the detector at the time of this particular observation. However, the linearity between the intensity of light and the output of the preamplifier was checked to be correct even under this condition.

V. DISCUSSION

Experimental results have proved that the radiation from a limited trajectory in gas in the millimeter-wave region shows the property of transition radiation even when the Čerenkov criterion $\beta n > 1$ is fulfilled, and that the Čerenkov threshold $\beta n = 1$ loses its practical meaning.

In radiation processes such as transition radiation and Čerenkov radiation from a limited trajectory of high-energy particles, the length L_f of the formation zone of Eq. (2.8) is significant. The formation zone is interpreted as the electron trajectory length required for the formation of radiation in the reference system of the electron moving with velocity βc relative to the laboratory system.

It is generally known that any type of radiation is not emitted from a point but from a finite region whose size is of the order of the wavelength of the radiation [21,22]. In other words, for the completion of a radiation process a time interval for the radiation to propagate a distance of one wavelength is required. We call it the formation time. The frequency ν' of radiation in the electron's reference system is given by the relativistic Doppler effect derived from the Lorentz transformation [23]:

$$\nu' = \gamma|1 - \beta n \cos\theta|\nu, \tag{5.1}$$

where γ is the Lorentz factor $\gamma = (1 - \beta^2)^{-1/2}$. The formation time in the electron's reference system is written as $\Delta t' = 1/\nu'$. Since the formation time Δt in the laboratory system is given as $\gamma\Delta t'$ by the Lorentz transformation, the distance the electron moves during the formation time Δt is

$$\Delta t\beta c = \frac{\gamma\beta c}{\nu'} = \frac{\beta c/\nu}{|1 - \beta n \cos\theta|}. \tag{5.2}$$

Since c/ν is equal to the wavelength λ in vacuum, the distance calculated above is the length L_f of the formation zone given by Eq. (2.8). Thus the formation zone expresses the length which is required to complete the radiation process. The values of L_f in this experiment are summarized in Table IV. In the millimeter-wave region the length L of this experiment is much shorter than the

length L_f of the formation zone.

On the basis of the role of the formation zone, we propose a new criterion $L > L_f$ for Čerenkov radiation. Using Eq. (2.8) and $\beta n > 1$, we obtain

$$\beta(n\cos\theta - \lambda/L) > 1, \tag{5.3}$$

instead of the conventional Čerenkov criterion $\beta n > 1$ for free space.

For the gaseous medium ($n \simeq 1$) and for the high-energy electrons ($\beta \simeq 1$), the Čerenkov angle θ_c is close to zero. When the acceptance angle of radiation covers the Čerenkov angle and $\theta = 0$ rad, the strictest criterion for gas is given by

$$\beta(n - \lambda/L) > 1. \tag{5.4}$$

This is equivalent to the criterion proposed by Zrelov *et al.* [4], which is derived from results of their numerical calculations. Their derivation is based on the consideration that the intensity of Čerenkov radiation should be proportional to the emission length.

Obviously, the difference between the conventional criterion for the free space ($\beta n > 1$) and the new criterion of Eq. (5.4) becomes important in the long-wavelength region where λ/L has a significant value compared with the refractive index n. In the case of a gaseous medium whose refractive index is close to unity, such as in this experiment, a finite value of λ/L is meaningful, even if it may be small.

In order to visualize the new criterion, the theoretical intensity calculated by Eq. (2.1), which is integrated over the acceptance angle and per bandwidth of 1%, is shown in Fig. 8 by a surface of a grid as functions of both λ/L and βn. This three-dimensional figure shows the property of the radiation from a limited trajectory. When λ and L are constant, it gives the relation between the intensity and the refractive index n as described in Sec. IV A. An example is shown by the dotted curve in Fig. 8. When L and n are constant, it shows the spectra as described in Sec. IV D, and an example is shown by the broken curve in the figure. When λ and n are constant, it gives the relation between the intensity and L as described in Sec. IV C.

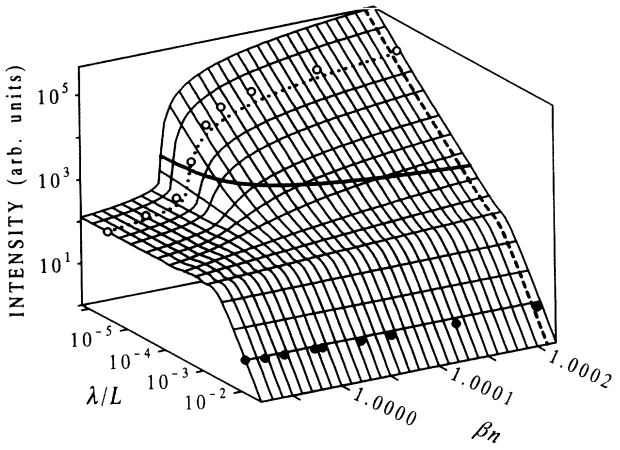

FIG. 8. Three-dimensional plot of the theoretical intensity of radiation emitted from a limited trajectory as functions of both λ/L and βn. The dotted curve shows an example of the pressure dependence of intensity at a constant wavelength. The broken curve is an example of spectral distribution of intensity at a constant pressure. The bold solid curve represents the threshold $\beta(n - \lambda/L) = 1$ of the new criterion on the grid. The open and the solid circles, respectively, show the observed values of the pressure dependence of intensity at $\lambda = 500$ nm and $\lambda = 2$ mm for the KURRI Linac in Fig. 4(b).

The bold solid curve in Fig. 8 represents the lower limit $L = L_f$ at $\theta = 0$ rad, i.e., $\beta(n - \lambda/L) = 1$, of the new criterion on the surface of the grid. The upper side of this curve is the region where the new criterion $\beta(n-\lambda/L) > 1$ is fulfilled. The open and the solid circles, respectively, show the observed values of Fig. 4(b) at $\lambda = 500$ nm and $\lambda = 2$ mm from the KURRI Linac. The values at $\lambda = 500$ nm in the visible region cross both curves $\beta n = 1$ and $\beta(n - \lambda/L) = 1$ when the value of n increases. On the other hand, the observation at $\lambda = 2$ mm in the millimeter-wave region does not satisfy the new criterion $\beta(n - \lambda/L) > 1$, though the criterion $\beta n > 1$ for the free space is fulfilled.

Therefore the radiation from a limited trajectory whose length does not satisfy the new criterion should be called transition radiation, even if $\beta n > 1$. In order to generate Čerenkov radiation in a gas in the long-wavelength region by high-energy electrons, we have to prepare an electron trajectory of several tens of meters or more because of the long length of the formation zone.

ACKNOWLEDGMENTS

We express our gratitude to Professor Y. Kondo of the Faculty of Engineering, Tohoku University, and Professor H. Yamaoka of the Research Reactor Institute, Kyoto University for useful discussions. We also thank T. Tsutaya of the Research Institute for Scientific Measurements, Tohoku University, A. Kurihara, S. Takahashi, and Y. Shibasaki of the Laboratory of Nuclear Science, Tohoku University, and the staff of the Research Reactor Institute, Kyoto University for their technical support and assistance. This work was partially supported by a Grant-in-Aid for Scientific Research from the Ministry of Education, Science and Culture of Japan.

APPENDIX: THEORY OF COHERENCE EFFECT IN THE MILLIMETER-WAVE REGION

In the millimeter-wave region the radiation intensity from an electron beam is usually weak and its observation is difficult. In recent years coherent radiation has been observed which is emitted from short bunches of relativistic electrons from a linear accelerator [10–12,16,18,24,25]. The power of the radiation in the long-wavelength region is enhanced enormously by the coherence effect.

The intensity of coherent radiation is given by [26]

$$P = \left| \sum_{j=1}^{N} \mathbf{E}_j \exp\left(i2\pi \frac{\mathbf{n} \cdot \mathbf{x}_j}{\lambda}\right) \right|^2 , \tag{A1}$$

where N is the number of electrons in a bunch, $\mathbf{E}_j$ the electric vector of radiation from the jth electron, $\mathbf{x}_j$ the position vector of the jth electron, and $\mathbf{n}$ the unit vector along the direction of observation.

The degree of the coherence effect depends not only on the longitudinal size of the bunch but also on the emittance, or the transverse size and the angular divergence, of the electron beam [16,26]. We assume that the distribution of electrons in a bunch has cylindrical symmetry. Then, Eq. (A1) is calculated as [26,27]

$$P = N\ (1 + N\, f_L\, f_T\, \chi)\ P_0, \tag{A2}$$

where f_L is a longitudinal bunch form factor, f_T a transverse one, and χ a factor of an electron-beam divergence. The number N is assumed to be much larger than unity. The function P_0 is the intensity of radiation emitted from a single electron and corresponds to P_0 of Eq. (2.1) or P_0^T of Eq. (2.7). The values of the factors f_L, f_T, and χ vary from zero (incoherence limit) to unity (coherence limit). With the minimum and maximum values of these factors, Eq. (A2) is reduced to

$$P = \begin{cases} N P_0 & \text{(incoherence limit)} \\ N^2 P_0 & \text{(coherence limit).} \end{cases} \tag{A3}$$

In circular cylindrical coordinates (ρ, ϕ, z) where the z axis is along the trajectory of the electron beam, the form factors are expressed as [26]

$$f_L = \left| \int h(z) \exp\left(\frac{i2\pi z \cos\theta}{\lambda}\right) dz \right|^2 , \tag{A4}$$

$$f_T = \left| \iint g(\rho) \exp\left(\frac{i2\pi\rho \sin\theta \cos\phi}{\lambda}\right) \rho\, d\rho\, d\phi \right|^2 , \tag{A5}$$

where $h(z)$ and $g(\rho)$ are the longitudinal and transverse density distribution functions of electrons in the bunch.

The divergence factor is derived from synthesis of vectors as

$$\chi = \left| \int \mathbf{e}\, G(\mathbf{u})\, d\mathbf{u} \right|^2 , \tag{A6}$$

where $\mathbf{e}$ is the unit vector of an electric field of radiation, $\mathbf{u}$ the unit vector of the direction of motion of an electron, and $G(\mathbf{u})$ the density distribution function of $\mathbf{u}$ in a bunch. In polar coordinates, Eq. (A6) is written as

$$\chi = \left\{ \iint \frac{\sin\theta\cos\xi - \cos\theta\sin\xi\cos\phi}{\sin\tau} G(\xi) \sin\xi\, d\xi\, d\phi \right\}^2 , \tag{A7}$$

where ξ is the polar angle of $\mathbf{u}$ and τ is the angle between the direction of motion $\mathbf{u}$ and the direction of observation $\mathbf{n}$.

Since the direction of radiation from relativistic electrons is mostly confined in a small angle (θ) along the trajectory of the electron beam, $\cos\theta$ is close to unity. Then, f_L of Eq. (A4) depends only on the wavelength λ and its value mainly determines the enhancement of the radiation intensity due to the coherence effect. On the other hand, since the values of f_T of Eq. (A5) and χ of Eq. (A7) depend greatly on the angle θ, the angular distribution of P in Eq. (A2) for coherent radiation is different from that of P_0 for the radiation emitted from a single electron.

For the theoretical calculations in this paper, the transverse distribution of electrons $g(\rho)$ and the distribution of the angular divergence $G(\xi)$ are assumed to be Gaussian functions as follows:

$$g(\rho) = \frac{1}{\pi\sigma^2} \exp\left(-\frac{\rho^2}{\sigma^2}\right) , \tag{A8}$$

$$G(\xi) = \frac{1}{\pi\Psi^2} \exp\left(-\frac{\xi^2}{\Psi^2}\right) , \tag{A9}$$

where σ and Ψ are the root-mean-square spread of the Gaussian functions. On the other hand, when we consider the relative values of the intensity in this paper, f_L is taken as unity for convenience.

The emittance ε_m is defined as $\varepsilon_m = \pi\sigma\Psi$ with the transverse size and the angular divergence of the electron beam when $g(\rho)$ and $G(\xi)$ are Gaussian functions. For the relativistic electrons the normalized emittance $\varepsilon_n = \pi\beta\gamma\sigma\Psi$ is used, where $\gamma = (1 - \beta^2)^{-1/2}$ [28].

[1] I. E. Tamm and I. M. Frank, Dokl. Akad. Nauk SSSR **14**, 107 (1937).
[2] I. E. Tamm, J. Phys. (Moscow) **1**, 439 (1939).
[3] J. D. Lawson, Philos. Mag. **45**, 748 (1954).
[4] V. P. Zrelov, M. Klimanova, V. P. Lupiltsev, and J. Ružička, Nucl. Instrum. Methods **215**, 141 (1983).
[5] V. P. Zrelov, V. P. Lupiltsev, and J. Ružička, Nucl. Instrum. Methods Phys. Res. Sect. A **270**, 62 (1988).
[6] D. K. Aitken, R. E. Jennings, A. S. L. Parsons, and R. N. F. Walker, Proc. Phys. Soc. London **82**, 710 (1963).
[7] I. M. Frank and V. L. Ginzburg, J. Phys. (Moscow) **9**, 353 (1945).
[8] J. R. Neighbours, F. R. Buskirk, and A. Saglam, Phys. Rev. A **29**, 3246 (1984).
[9] J. Ohkuma, S. Okuda, and K. Tsumori, Phys. Rev. Lett. **66**, 1967 (1991).
[10] Y. Shibata, K. Ishi, T. Takahashi, F. Arai, M. Ikezawa, K. Takami, T. Matsuyama, K. Kobayashi, and Y. Fujita,

Phys. Rev. A **44**, 3449 (1991).
[11] U. Happek, A. J. Sievers, and E. B. Blum, Phys. Rev. Lett. **67**, 2962 (1991).
[12] T. Takahashi, Y. Shibata, F. Arai, K. Ishi, T. Ohsaka, M. Ikezawa, Y. Kondo, T. Nakazato, S. Urasawa, R. Kato, S. Niwano, and M. Oyamada, Phys. Rev. E **48**, 4674 (1993).
[13] V. L. Ginzburg and V. N. Tsytovich, *Transition Radiation and Transition Scattering* (Adam Hilger, New York, 1990), Sec. 2.2.
[14] H. Ehrenreich, H. R. Philipp, and B. Segall, Phys. Rev. **132**, 1918 (1963).
[15] L. Wartski, S. Roland, J. Lasalle, M. Bolore, and G. Filippi, J. Appl. Phys. **46**, 3644 (1975).
[16] Y. Shibata, K. Ishi, T. Takahashi, T. Kanai, F. Arai, S. Kimura, T. Ohsaka, M. Ikezawa, Y. Kondo, K. Kato, S. Urasawa, T. Nakazato, S. Niwano, M. Yoshioka, and M. Oyamada, Phys. Rev. E **49**, 785 (1994).
[17] V. L. Ginzburg and V. N. Tsytovich, *Transition Radiation and Transition Scattering* (Adam Hilger, New York, 1990), Sec. 2.4.
[18] K. Ishi, Y. Shibata, T. Takahashi, H. Mishiro, T. Ohsaka, M. Ikezawa, Y. Kondo, T. Nakazato, S. Urasawa, N. Niimura, R. Kato, Y. Shibasaki, and M. Oyamada, Phys. Rev. A **43**, 5597 (1991).
[19] R. Gatto, H. M. Georgi III, A. D. Jackson, P. V. Landshoff, C. Mahaux, L. Montanet, J. P. Schiffer, R. H. Siemssen, and K. Winter, Phys. Lett. B **204**, 65 (1988).
[20] H. Hayano, M. Kikuchi, T. Naito, J. Urakawa, M. Yoshioka, T. Nakazato, M. Oyamada, S. Urasawa, and T. Yamakawa (unpublished).
[21] V. L. Ginzburg and V. N. Tsytovich, *Transition Radiation and Transition Scattering* (Adam Hilger, New York, 1990), Sec. 1.2.
[22] L. D. Landau and E. M. Lifshits, *The Classical Theory of Fields* (Pergamon Press, Oxford, 1975), Sec. 58.
[23] E.g., W. Pauli, *Theory of Relativity* (Pergamon Press, New York, 1958), Sec. 6.
[24] Y. Shibata, K. Ishi, T. Takahashi, T. Kanai, M. Ikezawa, K. Takami, T. Matsuyama, K. Kobayashi, and Y. Fujita, Phys. Rev. A **45**, 8340 (1992).
[25] T. Nakazato, M. Oyamada, N. Niimura, S. Urasawa, O. Konno, A. Kagaya, R. Kato, T. Kamiyama, Y. Torizuka, T. Nanba, Y. Kondo, Y. Shibata, K. Ishi, T. Ohsaka, and M. Ikezawa, Phys. Rev. Lett. **63**, 1245 (1989).
[26] L. A. Vardanyan, G. M. Garibyan, and C. Yang, Izv. Acad. Nauk Arm. SSR Fiz. **10**, 350 (1975).
[27] Y. Shibata, T. Takahashi, T. Kanai, K. Ishi, M. Ikezawa, J. Ohkuma, S. Okuda, and T. Okada, Phys. Rev. E **50**, 1479 (1994).
[28] E.g., M. Conte and W. W. MacKay, *An Introduction to the Physics of Particle Accelerators* (World Scientific, Singapore, 1991), Sec. 5.